Mixing and segregation of wheat bran and vegetables pieces binary mixtures in fluidized and fluid-spout beds for atomospheric freeze-drying

PREPRINT

of the paper

Coletto M.M., Marchisio D.L. and Barresi A.A.

Mixing and segregation of wheat bran and vegetables pieces binary mixtures in fluidized and fluid-spout beds for atmospheric freeze-drying

Published on *Drying Technology* **35**(9), 1059-1074 (2017)

[DOI: 10.1080/07373937.2016.1230741]

[online 4/10/2016]

Available at https://doi.org/10.1080/07373937.2016.1230741

Mixing and segregation of wheat bran and vegetables pieces binary mixtures in fluidized and fluid-spout beds for atmospheric freeze-drying

Mauricio M. Coletto*, Daniele L. Marchisio and Antonello A. Barresi

Dip. Scienza Applicata e Tecnologia, Politecnico di Torino, Corso Duca degli Abruzzi 24, 10129 Turin, Italy

Abstract

The segregation of binary mixtures of non-food wheat bran and vegetables at different levels of dryness was studied by simulating different stages of the atmospheric freeze drying by immersion in an adsorbent material (AFD IAM) process. It was characterized using a new set of four indices, which allows to evaluate not only the segregation level, but also the segregation pattern. The mixing performance was evaluated in a fluidized bed (considering also the effect of air superficial velocity) as well as in a spout-fluid bed, and peas, carrot discs, and potato slabs were used as food products. In general, it was found that food material segregates towards the bed bottom during the firsts stages of the drying process in fluidized beds, which translates in a poor contact product-adsorbent. On the contrary, uniform mixing patterns were observed in the spout-fluid bed, for the beginning and final stages of the process.

On the other hand, despite the very low cost of non-food wheat bran and its compatibility with food materials, it presents a channeling fluidization as a consequence of the cohesive properties of its particles. This behavior was also characterized by means of video analysis in two different fluidized beds. A channel generation and collapse general cycle was highlighted, whose frequency and channel characteristics depend on the air superficial velocity. In addition, three main types of food particle transport were identified: passive (downward),

*Corresponding author. E-mail address: mauricio.coletto@polito.it, currently at Departamento de Química, Universidad Nacional del Sur, Av. Alem 1253, B8000CPB Bahía Blanca, Argentina.

active (upward), and particle blocking effects. These findings allowed to explain segregation phenomena in these kinds of binary mixtures.

Keywords: segregation, binary mixtures, spout-fluid bed, atmospheric freeze drying, cohesive powder

1. INTRODUCTION

Binary mixtures occur frequently in the food industry, and their complex behavior can make handling difficult, reducing the efficiency of the process or impacting on the final quality of the product. Atmospheric Freeze Drying by Immersion in an Adsorbent Material in a fluidized Bed (AFD-IAM-FB) is one of the cases in which food technology faces with technical difficulties.

In general terms, in the lyophilization process (also known as freeze-drying) previously frozen material is dried by means of ice sublimation at low temperature. Normally, a primary drying stage for removing frozen water is followed by a secondary drying for evaporating the remaining bounded water. Basically, this process can be performed either at atmospheric pressure (atmospheric freeze drying, AFD) [1], or under vacuum (vacuum freeze drying, VFD) [2, 3]. In the second case it is essential that the water partial pressure is maintained at very low values, below ice vapor tension, to allow sublimation, but the freeze-drying might be combined with the application of microwaves [4, 5], ultrasound [6, 7], and various other methods to enhance and/or accelerate drying, as it was described in a extensive review by Pisano *et al.* [8].

AFD has been getting importance in the last years for industrial food applications, as a consequence of its relatively reduced operating costs and the higher quality of the final products compared with that obtainable with conventional drying. Many authors have been working on this process during the last three decades,

investigating different factors affecting heat and mass transfer, improving them with some extra energy supply, and/or evaluating final product quality from the point of view of shape, color, or rehydration capacity (see for example [9, 10, 11, 12, 13]. In addition, different types of equipment were also proposed to carry out atmospheric freeze-drying, ranging from tunnel driers or fixed beds to fluidized beds, either standard, vibro or pulsed [14, 15, 16].

Duan *et al.* [17] reviewed recent literature on freeze drying considering not only the available techniques for freeze-drying up to now, but also the effect of temperature on generated pores during the drying process and its results on product quality, energy costs and efficiency, and highlighted the main features and process control strategies of microwave assisted freeze-drying, AFD, and VFD.

In particular, various researchers have investigated the main variables influencing the AFD in fluidized beds. However, this process is usually carried out with air at temperatures between -15 and -5 °C, which therefore can reach saturation rapidly. This situation leads to a reduction of the gradient of water concentration between the air and the product surface, and consequently, to a diminution of the mass transfer rate. AFD-IAM may thus be a good technical solution to maintain a low water partial pressure in the air along all the bed. Moreover, the use of the adsorbent medium presents two additional advantages: first, as the heat of adsorption of water vapor is of the same order of magnitude of the sublimation heat of ice, no additional energy supply is necessary; second, it acts as an adsorbent medium for the generated water vapor, allowing to recirculate the drying air, which means an additional reduction of operating costs.

Donsì *et al.* [18] investigated the influence of many factors, such as freeze drying temperature, fluidization velocity, nature of adsorbent material, size of adsorbent particles, and product/adsorbent weight ratio, on the final drying rate, employing different materials as adsorbent and potato discs as product. It was found that the

fluidization velocity has no important effect on the drying rates and at high product concentration the foodstuff segregates, leading to poor contact with the adsorbent. Further results by Di Matteo [19] evidenced that at lower product concentrations the drying process takes place more rapidly, in other words, the product absolute humidity (kg_{water}/kg_{dry}) decreases faster. However, product to adsorbent ratios less than 1/20 have no significant effects on augmenting the drying velocity as the processes is controlled by external mass transfer during the first period only.

Wolff and Gibert [20] developed a model for the simulation of atmospheric freeze drying processes, under certain assumptions. They carried out some experiments that reflected the influence of parameters such as temperature, water content, product to adsorbent mass ratio, shape and size of the product to be dehydrated, and temperature for adsorbent regeneration. They used potato slices as product and starch as adsorbent. Nevertheless, the authors did not mentioned whether segregation phenomena or formation of channels were present or not.

Due to its compatibility with food products and very low price, since it is a by-product of wheat processing, non-food wheat bran seems to be a promising material to be used for AFD. Nonetheless, as it is the hard outer layer of cereals consisting of combined aleurone and pericarp, obtained as a by-product of milling in the production of refined grains, its particles exhibit a very irregular plane shape, with rests of grain brush and, in some cases, broken pericarp. These characteristics confer to the particles a rough surface and, as undesired consequence, the possibility of mechanical interaction during fluidization.

In addition, when AFD-IAM-FB is evaluated it is important to consider not only the interplay between particles of the adsorbent phase, but also the interaction between food pieces and adsorbent. In other words, segregation phenomena should be taken into account in this case, as two particulate systems of completely different size and density are fluidized in the same bed.

According to Rowe *et al.* [21] (who investigated bubbling fluidized beds of non-cohesive materials), density differences are the main causes of segregation in gas fluidized beds, whereas size differences have a slight influence when the mixture is made up of particles of equal density and different size. Moreover, working with mixtures composed of solids of different densities, Qiaoquna *et al.* [22] observed that an increment on the mixture mean diameter, by means of either augmenting the overall mass fraction of the larger particles or using particles with greater diameter for one of the phases, increases the mixture minimum fluidization velocity. This results in a reduction of air excess velocity, and consequently, the segregation of the particulate system is potentiated.

Regarding fluidization time, the minimum elapsed time required to reach segregation equilibrium depends on the excess velocity used and larger to smaller particle diameter ratio. For excess air velocities greater than 0.16 m/s, 20 minutes were found sufficient to achieve good mixing. Moreover, the same fluidization time is sufficient for diameter ratios up to 4.8 [23].

One of the main mixing factors in non-cohesive systems are air bubbles, which carry particles in their wakes. The number and size of bubbles might depend on air velocity, and particle size distribution (PSD) [24]. Nonetheless, mixing and segregation in cohesive or pseudo-cohesive systems (which share characteristics of cohesive and non-cohesive powders) may be affected by different factors rather than bubbles, such as channel generation and collapse.

In order to obtain a better understanding of the segregation phenomenon it is important to study the fluid-dynamics of the fluidized beds, and the behavior of the components of the mixture during fluidization. Considering the density and Sauter's diameter of the powder particles, its most probable behavior in a fluidized bed can be predicted referring to its Geldart's classification [25]. However, some powders like non-food wheat bran, may be classified into a given category according

to their density and diameter, but may behave differently because of their physical characteristics described above. Another important indicator of the dynamics of a fluidized bed are the pressure drop oscillations. They depend on particle properties, bed characteristics, and air velocity, and might be related to bubbling, slugging, or turbulent fluidization [26].

In the fluidization of cohesive powders the inter-particle forces are greater than the drag forces leading to the formation of plugs in small diameter fluidized beds and channels in larger ones. These inter-particle forces may be caused by either electrostatic charges or liquid bridges (wet or sticky materials) [25]. In particular, the main cohesive forces between particles in a powder are van der Waals forces, which can be perceived only by very small particles (few microns or less), depending on the particle density, porosity and surface roughness [27]. On the other hand, an increment on the moisture level of the bed results in an increase of the inter-particle forces due to liquid bridges, causing a reduction of the bed expansion at low gas velocities but its rise at high velocities [28]. Moreover, particles may link together in layer/plate structures resulting in a extra frictional forces with the bed walls, increasing the pressure drop during the packed-bed regime [29]. Further information and discussions about this pressure overshoot and other factors involved in cohesive fluidization can be found in an exhaustive review paper published by Sundaresan [30]. In addition, the cohesive forces can be approached by mathematical models taking into account the formation of agglomerates and effective agglomerate diameter as done by Zhou and Li [31] and van Wachem and Sasic [32].

An improvement of the material circulation and solid mixing can be obtained by considering different kinds of beds for AFD-IAM. The “spout-fluid bed” (a modified spouted bed with auxiliary air injectors located in the lower section of the bed) seems to be an interesting example, as it presents better solids mixing and annular solid-fluid contact than standard spouted beds, and better performance when cohesive

solids are used [33]. Though, the particle diameter ratio has a pronounced effect on segregation even for these kinds of beds, particularly for Geldart D glass beads, reducing the mixing degree of the binary mixture as the size difference increases [34, 35, 36]. On the contrary, particle density differences seems to exert a reduced effect on segregation using high air velocities in the main injector [37].

Additionally, many works can be found in literature on spout-fluid beds, evaluating their characteristics as drying apparatus [38, 39], investigating in particular their hydrodynamics [40], their fluidization regimes [41, 42], developing correlations for predicting fountain height, and discussing modeling aspects [43, 44].

Most of the previously mentioned works and other papers found in literature were carried out using non-cohesive powders forming binary mixtures whose components had diameters not greater than one or two millimeters. Besides, in most of the cases spherical or nearly spherical particles were utilized in the mixtures. Therefore, there is a lack of information about the behavior of fluidization of binary mixtures of a cohesive or pseudo-cohesive solid and not spherical particles with equivalent diameters in the order of centimeters, and in particular there is a lack of knowledge about how a pseudo-cohesive powder like non-food wheat bran works in a fluidized bed or a fluid-spouted bed, its behavior as component of binary mixtures with particles up two orders of magnitude greater, and the link between channeling and mixing.

Therefore, a deeper study about the characteristics of this very cheap material and its hydrodynamic interactions with food particles should be performed before investigating the AFD of food applying it as adsorbent.

On the other hand, a particular approach to mixing/segregation indices is needed allowing a more precise quantification of the segregation phenomenon and comparison between different beds.

The main objective of the present work is twofold: on one hand to characterize

the hydrodynamic behavior of non-food wheat bran, as potential adsorbent for AFD IAM in fluidized bed as well as spout-fluid bed; on the other hand to study the segregation of binary mixtures of non-food wheat bran and vegetables at different level of dryness simulating what happen during the drying process, and to establish the ideal conditions under which AFD IAM can be performed without excessively reducing the product size.

Fluidized beds will be investigated in detail, but very strong segregation problems will be evidenced in this type of apparatus, while spout-fluid beds appear as the suitable technology for uniform fluidization. The segregation mechanisms occurring in this type of beds will be also deeply investigated, to evidence differences with respect to bubbling fluidized beds.

2. MATERIALS AND METHODS

2.1. Food material and adsorbent

Knowing the non-food wheat bran absolute density (1469 kg/m^3) and its minimum fluidization velocity (0.17 m/s) obtained from preliminary experiments, an Equivalent Diameter for Fluidization (EDF) was estimated by solving the Ergun's equation for the particle diameter:

$$0 = \frac{1650 u_{\mathrm{mf}} \mu}{g} \frac{1}{d_{\mathrm{eq}}^2} + \frac{24.5 u_{\mathrm{mf}}^2 \rho_{\mathrm{air}}}{g} \frac{1}{d_{\mathrm{eq}}} + (\rho_{\mathrm{air}} - \rho_{\mathrm{A}}) \quad (1)$$

which was estimated to be 626.6 µm.

Then, according to this information and the absolute density, it was classified as B Type in the Geldart's classification of powders [25]. Moreover, from image analysis the bran particle thickness was determined to be around 140 µm.

Another salient characteristic of non-food wheat bran obtained from sieving analysis and estimation of the Sauter diameter of each class, is that about 90 % of

particle population belongs to Geldart B group, and only approximately 10 % to Geldart A. In other words, the presence of Geldart C (cohesive) particles is negligible.

Fresh food material was purchased in the local market, and cut in discs, slabs, or cubes (Table 1). Lyophilized material was obtained by vacuum freeze drying in a small-size industrial apparatus (*LyoBeta 25*^{TM} by Telstar, Terrassa, Spain), by using the same conditions for every food material.

2.2. *Experimental apparatus*

According to the characteristics of each experiment series, different fluidized beds were utilized. Table 2 presents the utilized beds, their characteristics, and the experiment types carried out in each one. In all the cases air at ambient temperature was used (about 25 °C).

In both L35b (Figure 1(a)) and L20b fluidized beds, air is injected into the bed via a gas distributor consisting of a square perforated plate. The hybrid spouted bed (fluid-spout bed) has, added to its central air jet, lateral air injectors situated at the bed bottom (Figure 1(b)), which help to avoid the accumulation of larger material at the bed bottom. In the figure it is evidenced the position of the distributor screw as it can have an effect on the product quality as it will be discussed in the results section.

During preliminary fluidization tests it was found that the utilized bran fluidizes more like a cohesive powder rather than a Geldart B one. Thus, aiming to obtain a qualitative description and quantitative data about the fluidization behavior of a binary mixture (containing non-food wheat bran) in the 35 cm sided fluidized bed, videos were taken while doing fluidization experiments, through its Plexiglas window (camera *Panasonic DMC-TZ4*, video mode, 25 frames/second). Then, they were analyzed frame by frame and information about bed height, number of frontal channels, and the variation of these variables during the fluidization at different

velocities was taken. Only the number of frontal channels was considered, as it was quite complicated to measure the total number of channels. However, by visual inspection in the L35b fluidized bed, it was observed that this variable is proportionally representative of the number of channels in the rest of the bed at 1.5 and 1.7 times the adsorbent minimum fluidization velocity (u_{mfA}).

Another series of experiments was performed in the geometrically similar L20b fluidized bed using binary mixtures. Also in this case videos were taken through the bed Plexiglas frontal wall for frame by frame analysis. These experiments were done with the scope of obtaining a general idea about the behavior of channels formation and solid phases interaction. Although there would be some differences concerning to channels length, or their diameters between the two beds, the main idea was to better observe the channeling phenomenon already seen in the upper part of the 35 cm sided bed.

Furthermore, in order to obtain better information about the pressure drop during channel generation and collapse of wheat bran, experiments in a small Plexiglas 65 mm diameter cylindrical bed (L065b) were carried out, measuring pressure drop using a water manometer. The small diameter of the fluidized bed was particularly chosen because it allows the formation of only one channel with the used wheat bran. Videos were taken in this case as well.

2.3. Mixing and segregation experiments

Different binary mixtures containing bran and lyophilized food materials were utilized to evaluate the effect of particle shape, food concentration, fluidization time, food density and air velocity on segregation. In order to eliminate the dependence on the initial mixture state and to highlight the influence of previous parameters, these experiments were mainly carried out loading initially homogeneously mixed binary mixtures; but a series of experiment was also carried out starting with

non-homogeneously mixed mixtures.

The homogeneous mixtures were previously prepared by equally dividing the total amount of food material and adsorbent in few smaller quantities. They were separately mixed and, finally, gradually loaded one by one into the fluidized bed (in the L035b, through the Plexiglas window when possible or a lateral removable window near the top; in the L020spjet, directly from the top).

Segregation was evaluated by means of a novel index set, the Three Thirds Segregation Index Set (TTSIS), consisting of three numbers that evaluate the distribution profile of a material of interest (food product, for the current case) and a fourth one that gives an idea of the segregation level. The first index is the Bottom Third Indicator, the second one is the Middle Third Indicator, the third one is the Top Third Indicator, and the last one is the Segregation Level. These indices are respectively labeled as p_{I} , p_{M}, p_{S}, and $\aleph_2$, and together are expressed as $[p_{\mathrm{I}}, p_{\mathrm{M}}, p_{\mathrm{S}}]_{\aleph_2}$.

Considering h^* as the dimensionless position in the bed from the bottom (calculated as the ratio of the height in the bed from the bottom and the total bed height in settled state), and defining $F_{\mathrm{q}}(h^*)$ the accumulated mass of material of interest "q" as a function of h^*, these three indicators are calculated as follows:

$$p_{\mathrm{I}} = \frac{F_{\mathrm{q}}\left(\frac{1}{3}\right)}{m_{\mathrm{qT}}} \tag{2}$$

$$p_{\mathrm{M}} = \frac{F_{\mathrm{q}}\left(\frac{2}{3}\right) - F_{\mathrm{q}}\left(\frac{1}{3}\right)}{m_{\mathrm{qT}}} \tag{3}$$

$$p_{\mathrm{S}} = \frac{m_{\mathrm{qT}} - F_{\mathrm{q}}\left(\frac{2}{3}\right)}{m_{\mathrm{qT}}} \tag{4}$$

and

$$\aleph_2 = \max(p_{\mathrm{I}}, p_{\mathrm{M}}, p_{\mathrm{S}}) - \min(p_{\mathrm{I}}, p_{\mathrm{M}}, p_{\mathrm{S}}) \tag{5}$$

Based on the values obtained with the TTSIS, different segregation patterns can be identified (i.e. Full Top, Uniform, Bottom Central). Further information on experimental determination of above parameters, about the extreme and intermediate values of TTSIS, and criteria utilized for classification of the segregation patterns can be found in previous works [45, 46]. Additional details, performance analysis and comparison with other mixing indices can be found in the cited thesis and article.

In order to investigate the food particles displacement during the fluidization, some of them were marked as tracers in some experiments. Two kinds of tracers were differentiated with different colors: Top Tracers (initially in the upper third of the bed), and Bottom Tracers (initially in the lowest third of the bed). TTSIS was also calculated for tracer particles, allowing an easy and simple description of the foodstuff movements during the process.

Furthermore, experiments in the spout-fluid bed (L20spjet) were carried out based on the results of the segregation experiments and the study of bran behavior during fluidization at different velocities. Only one concentration of food material was used (1/20 fresh product to bran mass ratio), and the maximum air velocity that does not cause the transport of bran and food material out of the bed, with 20 minutes of fluidization time, was applied.

Fluidization time and layer vacuuming

Except for experiments starting with inhomogeneous mixtures or special tests for evaluating the effect of time on segregation, the applied fluidization time was 20 minutes for experiments performed in the fluidized bed (L35b) as well as in the fluid-spout bed (L20spjet). This fluidization time was particularly chosen based on the work of Wu and Baeyens [23] and preliminary tests which have demonstrated that 20 minutes are enough for evidencing the effect on segregation of the studied variables. Once elapsed the selected fluidization time, the air supply was rapidly

shut off, then the mixture was collected in six layers by means of a vacuum cleaner and sieved. Adsorbent and food materials were weighed separately in order to determine their concentration in each layer.

In the experiments carried out in the L35b the material vacuuming was started through a window with a removable plate located at the middle-height of a lateral wall, and continued from the bed front by removing the Plexiglas window, while the vacuuming operation in the L20spjet was completely carried out from the bed top. On the other hand, the settled bed surface was quite irregular turning difficult to measure an exact value for the bed height (and consequently, the value of $h_{\mathrm{bed}}/6$). Thus, although during the vacuum operation the layer thickness was maintained as regular as it was possible for all layers, it was not possible to take precise direct measure for it. Thus, the dimensionless thickness of layer i was estimated as:

$$\Delta h_i^* = \frac{\Delta h_i}{h_{\mathrm{bed}}} = \frac{m_{\mathrm{A}i} + m_{\mathrm{P}i}}{m_{\mathrm{A}} + m_{\mathrm{P}}} \tag{6}$$

where m_{A} and m_{P} are the mass of adsorbent and product respectively.

Performed experiments and utilized nomenclature

Table 3 lists all the performed experiments in the L35b fluidized bed as well as in the spout-fluid bed (L20spjet), their ID, lyophilized material concentration, velocity, and air flow.

Based on the paper published by Donsì *et al.* [18], the chosen concentrations for experiments were, in terms of fresh product to adsorbent mass ratio, 1/20, 1/40, and 1/80.

Each experiment was identified with an alphanumeric code, such as *aaannnnRbb-tee*, where: *aaa* is the food material code (see Table 1); *nnnn* is the theoretical u/u_{mfA} multiplied by 100; *bb* is the reciprocal of fresh product to adsorbent mass ratio (for lyophilized material, the corresponding mass ratio for the original fresh product is

given); *ee* is the fluidization time in minutes.

3. RESULTS AND DISCUSSION

3.1. Non food wheat bran fluidization behavior

Unlike sand or other materials presenting formation of regular bubbles, wheat bran exhibits canalization or preferential air paths formation, without regular generation of bubbles. Moreover, even if the air superficial velocity is augmented up to about twice the bran minimum fluidization velocity, the bed expansion remains at around minimum fluidization value and air "in excess" escapes through channels without rising the bed.

Considering the non-food wheat bran particle size distribution, its EDF and absolute density, this powder cannot be classified as cohesive (Geldart C). Nevertheless, it behaves like a Geldart C powder in a fluidized bed. This contradiction can be explained taking into account the physical characteristics of the bran particles such as rough surface and remains of grain brushes, leading to mechanical interactions (rather than electrostatic forces). Therefore, this kind of powder might be called "pseudo-cohesive".

As discussed in the introduction, some works in the literature report changes in the fluidization behavior due to variations in the moisture content of the fluidized material such as a shift in the Geldart behavior (from B or A type, to A or A/C) and/or a reduction of the minimum fluidization velocity [29, 47, 48, 49, 50]. Nonetheless, taking into account the previous paragraphs, no significant effect of moisture content was assumed for non-food wheat bran, as the channeling behavior would be merely accentuated in the worst case.

Furthermore, the existence of three zones along the bed (top, middle and bottom) was observed in tests with the L20b fluidized bed. In the middle zone, there

are no channels and air simply percolates through it, whereas at top and bottom the generation and collapse of channels follows a quite regular cyclical behavior. However, depending on air superficial velocity the height of the middle zone can be very short (even null), or extend practically along all the fluidized bed. Despite these zones were observed only in the L20b fluidized bed, since its Plexiglas window completely covered one of its sides, their presence may be assumed for the L35b fluidized bed as well. Accordingly, segregation experiments by using potato slabs (POd) have demonstrated the existence of these three zones as damaged potato slabs were found in the bed bottom due to the agitation in this part of the bed, and their impossibility of rising the bed (see Section 3.2 for further information).

Channels Generation and Collapse General Cycle

Depending on air superficial velocity, only one big channel, few middle-size channels, or very few small ones might form in the bed. In general terms, a cyclical behavior of channels generation and collapse can be observed (as described in Figure 2). The number and shape of channels depend on air superficial velocity as well as on the position where they are formed in the bed. For example, by comparing the abscissas of Figures 3(a) and 3(b) it can be noted an increment on the oscillation frequency of bed height and channel generation and collapse as air superficial velocity is increased. In addition, a reduction of the average number of channels with increasing the mentioned variable can be observed. Hence, it can be said that this channeling behavior follows the general cycle showed in Figure 2 represented with two main stages: I, generation, and II, collapse.

Furthermore, from experimental observations, it can be said that the behavior of the channels generated in the upper part of the bed is comparable with that of a spouted bed (where three different regions, the annulus, the spout, and the fountain, are present) whose air velocity is varied. In other words, it can be compared with the

description given by Malek *et al.* [51] for the spout of a spouted bed as air velocity is raised. Therefore, the different phases of the Channels Generation and Collapse General Cycle are described as follows:

• **Abrupt pressure release:** It may take place either near the bed surface, originating a path after a burst (Figure 4, t = 49.0 s, square base 35 cm sided fluidized bed, L35b), or far from the bed surface generating an internal channel extending up to a roof of compacted material. In the former case, the channel behaves like a spouted bed where air velocity has overcome the minimum spouting air velocity and a fountain of material thrown appears over the spout. Pressure drop through the channel reaches a maximum and starts decreasing. Similarly occurs with air velocity inside the channel and fountain height reaching their maximum magnitudes. Inversely, bed height is minimum.

• **Phase I (Generation):** Pressure continues releasing, and new channels may appear as the result of the splitting of one single channel (Figure 4, from t = 54.2 s to t = 61.4 s). Simultaneously, material coming from other parts of the bed and/or collapsing channel walls starts blocking it until kinetic energy of coming out air is sufficient to drag the falling bran. If the channel is formed in the upper zone of the bed, a sudden decrement of fountain height can be seen. This situation is analogous to a spouted bed whose air velocity is progressively reduced after overcoming its minimum spouting velocity.

• **Phase II (Collapse):** Falling material blocks the channel orifice and air starts to be accumulated, increasing pressure below the material layer. When the pressure below the accumulated material is greater than the sum of the hydrostatic pressure caused by the plug and the forces embedding the material, a new abrupt air release takes place. In other words, the measured pressure drop continues reducing due to the increment of pressure inside the channel (unlike it would be expected in a spouted bed whose pressure drop remains almost constant during air velocity

reduction). In the case of upper channels, at the end of this phase, pressure drop as well as fountain height reach a minimum.

Thus, the layers above channels obstructing them constitute "weak zones" where the adsorbent is less compacted than the material in the surroundings. Nevertheless, not only the descending material in channel orifices can originate a "weak zone", but also the presence of another solid such as a food particle may induce it (Figure 5, from t = 91.8 s to t = 92.9 s, square base 20 cm sided fluidized bed, L20b).

More clear observations of the previously described cycle were done with experiments performed in the L065b bed (a snapshot of the most representative results is shown in Figure 6). Due to the geometric characteristics of the bed (small diameter, cylindrical, etc) and bran particularities (such as mechanical interactions between particles), only one channel was formed, allowing the measurement of pressure drop and height of thrown material of a single channel without possible interferences caused by other channels.

Based on the fact that the standard deviation of the pressure drop varies practically linearly with the gas superficial air velocity (meaning that if the latter is 0, the former will be approximately 0 as well), several authors established a threshold for determining whether a defluidization process is taking place or not. This value can be estimated either by visual observations and/or other methods such as statistical or frequency domain analysis [52, 53, 54].

In Figure 7 the standard deviations of the variables shown in Figure 6, estimated considering a moving time interval double of the average cycle time (calculated according to the criteria proposed by van Ommen *et al.* [55]), are presented. In the present case, neither by visual observations, nor by analyzing the bed height and height of thrown material in Figure 6, a defluidization process can be detected. In addition, correlating the curve of the standard deviation of the pressure drop with those of the bed height and height of thrown material, it can be inferred that no

defluidization occurs as their values are always larger than zero, meaning that bed material does not stop its movement. Therefore, no threshold can be established for defluidization.

On the other hand, the following observations can be made, evidencing the Channels Generation and Collapse General Cycle:

1. A sudden increment on the bed activity can be inferred from the increment of the standard deviations of the pressure drop and the thrown material in the "air burst" stage;
2. During Phase I of the cycle the standard deviation of all measured variables reduces indicating a diminution of the air velocity inside the channel (which causes a simultaneous decrease of h_{bed} and ΔP);
3. In Phase II the pressure drop is low while its standard deviation increases, which can be explained by an increment of the pressure inside the channel. Therefore, it can be said that the accumulated air inside the channel exerts a force on the upper bran particles which results in an increase of the bed height and the standard deviation of this variable.

On the other hand, analysis is much more complex in larger beds as several channels are simultaneously formed and generated at low air velocities while the bed is chaotically agitated at high air velocities, but at least some qualitative agreements were found and the behavior can be inferred from the transport mechanisms of food particles hereafter described.

3.2. Segregation of binary mixtures

In many works treating segregation and mixing, the concepts of *jetsam* (component tending to sink to the bed bottom) and *flotsam* (component tending to float to the bed top) introduced by Rowe *et al.* [21] are generally used. Nonetheless, as in the

binary mixtures considered in the present work the lighter component, the food product, is at the same time the larger one, it is not possible to establish *a priori* whether it will tend to sink or float. Hence, these terms will not be applied in the current discussion.

Figure 8(a) shows the segregation level as a function of the air superficial velocity to bran minimum fluidization velocity ratio for mixtures with partially and completely lyophilized material, whereas in Figure 8(b) is represented the segregation level as a function of the equivalent fresh product to adsorbent mass ratio. In addition, in Table 4 the other TTSIS indices of these experiments are summarized.

Results corresponding to experiments in the L35b with mixtures containing fresh food product are not presented neither in the figures nor in the tables since they exhibited Full Bottom segregation independently of air superficial velocity, product volume fraction, or food particle shape.

As it can be seen in Figure 8(a), for dried carrot discs (CAa and CAb cases) and dried potato slabs (POd cases) the segregation level increases with air superficial velocity until a peak is reached (which can be assumed between 1.7 and ≈ 2.4 u_{mfA}, depending on food material), and then it reduces to relatively low values at 2.6 u_{mfA}. Similarly, in Figure 8(b) carrot (CAa) cases show the maximum segregation level at 1.7 u_{mfA} (CAa0170) independently of product concentration. Nevertheless, lyophilized peas (PEa cases) present a completely different behavior; for this kind of binary mixtures the segregation level is reduced almost linearly as air velocity increases.

About partially lyophilized peas, they have to be maintained in frozen state in order to conserve their structure. This fact makes this material difficult to handle. Anyway, two experimental points were acquired, and it was observed that very high segregation levels where obtained for these experiments, as a consequence of the higher density of the partially dried material in comparison with the dried one.

Besides, it is interesting to remark that segregation levels obtained using binary mixtures containing potato slabs (POd) are considerably greater than values obtained employing mixtures with carrot discs (CAa, CAb), and values presented by mixtures containing peas (PEa, PEc) are notably lower than the other two binary mixtures. Therefore, since the difference in shape factor between carrot discs and peas is about 30 %, and between potato slabs and peas is about 50 %, it can be said that product sphericity plays a very important role on the mixing of this kind of binary mixtures. What is more interesting to note is that, in experiments carried out using POd, holey potato particles were found in the bed bottom, meaning that they descended but they could not ascend again due their planar and wide shape. Consequently, potato pieces hit over the bed distributor screw causing their perforation.

Concerning segregation profiles, as it can be seen in Tables 4 and 5, in general experiments at low and middle velocities (1.5-1.9 u_{mfA}) exhibited intermediate behaviors of Bottom segregation (Bottom, Bottom Central, Central Bottom, and V-Bottom). At high velocity (2.6 u_{mfA}) nearly Uniform profiles were obtained. In some cases at high velocity according to the classification criteria for segregation type, they are not uniform. However, not only the segregation type should be taken into account for evaluating the mixing, but also the segregation level: despite the segregation profile was not Uniform type, if the segregation level is low (approximately 0.15 or less), the distribution can be considered uniform to some extent.

In mixtures containing partially lyophilized peas (PEb), a predominant Bottom segregation and great segregation levels were found. Anyway, air velocity affects this last variable in the same way that in the other cases, reducing it.

Another experiment series where the influence of the air superficial velocity was highlighted is the one with lyophilized potato slabs (POa); particularly in the POa0170R40t10 case, starting with an induced Top segregation, a nearly uniform segregation pattern was obtained after fluidizing the bed at high air superficial

velocity. Also, the effect of product weight fraction on segregation is similar to CAa cases.

Regarding the effect of fluidization time, in Figure 9(a) it can be noted that as the time goes on the segregation profile changes from Central Top to Bottom at 1.5 u_{mfA}, and from Central Bottom to Bottom Central at 1.7 u_{mfA}, whereas at 2.6 u_{mfA} the segregation type is Uniform independently of elapsed time. Considering the TTSIS of tracer particles in the figure, at 1.5 u_{mfA} it can be observed that particles initially in the bed bottom (iB) remained there, while food particles initially in the bed upper third (iT) moved toward bed bottom. A similar but less pronounced situation can be noted for cases at 1.7 u_{mfA}. On the contrary, tracer particles at 2.6 u_{mfA} are distributed more uniformly. Thus, two main conclusions can be drawn: first, product particles displacement toward bed bottom prevails at low velocities, and second, the peaks observed in the segregation level at intermediate velocities discussed in previous paragraphs may be only transient situations, prevailing the Bottom segregation trend if fluidization time is increased.

For example, in case CAb0190R20t20 (Table 6) it can be seen that while the most part of the bottom tracers remained in the bed bottom, a great part of the top tracers descended to the bed middle and bottom thirds. A more pronounced situation can be noted for POd0150R20t20 and POd0170R20t20 cases, where practically all the bottom tracer remained in the bed bottom, and the greatest part of the top tracer particles was found in the lowest third of the bed.

On the other hand, a different distribution of the tracer particles can be observed for PEc cases, which are more uniformly distributed than tracers of CAb and POd. That would mean that the V-type of segregation profiles presented by mixtures containing this material might be also a transient stage. Thus, it might be asseverated that they may evolve to Uniform profiles as time goes on.

From experiments utilizing six binary mixtures combining materials with differ-

ent properties (density, size, and minimum fluidization velocity) in a two-dimensional fluidized bed, Rowe *et al.* [21] found four main segregation mechanisms, valid for bubbling fluidized beds. These mechanisms are based on the interaction of the materials with the bubbles (lifting in the bubbles wakes, or falling of denser and larger particles through their free space), and particle interactions (inter-particle percolation of smaller and denser particles through large and light ones, and quasi-hydrostatic effect, when lighter particles float on a bed of denser particles).

Unlike the cases where a binary mixture is fluidized in a bubbling fluidized bed and bubbles are the main mixing agent, in channeling fluidized bed the mixing might be attributed mainly to the shaking of the bed, and channels generation and collapse cycles. Thus, three main types of product particle movement mechanisms can be individuated: passive transport (downward), active transport (upward), and movement blocking, which only in part may be analogous or similar in some way to those described by Rowe. Moreover, the presence and frequency of these mechanisms depend upon air superficial velocity, and they often occur simultaneously in different parts of the bed.

In passive transport (Figure 10), adsorbent material below food particles is dragged by air through channel orifices and deposited on bed surface. Consequently, a downward motion of foodstuff takes place as a result of the collapse of the generated void under it. On the opposite, a food particle is actively transported when it is dragged by air and other bran particles through the channels in upward direction (see Figure 11; this mechanism may correspond to lifting of particles enclosed in rising bubble wakes which occurs in bubbling fluidized beds).

Additionally, as a result of interaction between adsorbent particles, two main effects causing particle blocking may be identified: floor effect and roof effect (Figure 10, t_3). The former is caused by agglomerates of embedded bran particles or more compacted zones avoiding the fall of product particles. The compaction

level decreases increasing air superficial velocity mainly because of a higher mobility in the fluidized bed. The latter blocking effect occurs when either a food particle is covered by adsorbent due to the collapse of a channel wall (Figure 10, t_3), or a layer of more compacted material is present above it, obstructing the possibility of ascendant movement. These effects may be considered the correspondent ones to the quasi-hydrostatic effects described by Rowe *et al.* [21], but are completely different in their causes.

At high velocities (2.3-2.6 u_{mfA}, 0.39-0.44 m/s) pressure release takes place through only one channel of large diameter. In each air burst, a fountain reaching fountain heights of about twice the bed height is generated (as it was presented in Figure 3). The Channel Generation and Collapse Cycle repeats at elevated frequencies, and food particles are actively transported by air and moving bran particles. At the same time, due to bed agitation, floor effect is practically absent allowing passive transport during channels collapse. Consequently, the lyophilized material uniformly distributes along the bed.

At intermediate velocities (1.7-1.9 u_{mfA}, 0.29-0.32 m/s), the number of channels often increases after a burst by splitting the original one. Though, air velocity inside them seems to be not sufficient for continuously dragging food material. Furthermore, due to the vibration of bran particles the floor effect is quite reduced and food particles sink. Moreover, during the second stage of the cycle, pressure has been completely released and the number of channels reduces due to collapse of their walls and material depositing over them. Thus, even if a channel were generated at bed bottom, food particles could not ascend due to roof effect. In particular, as it was previously said, in POd cases perforated potato particles were found in the bed bottom, where evidently particles are agitated and hit the distributor screw. More specifically, case POd0170R40 presented the maximum quantity of damaged food particles (about 44 %) among all experiments using POd.

At low velocity (1.5 u_{mfA}, 0.25 m/s) one or two small diameter channels are detected. A complete absence of channels in the second stage of the Channel Generation and Collapse Cycle is also possible. As a consequence of this practically lack of shaking, floor and roof effects are notably high avoiding food particles sinking and eventual ascendant movements. Therefore, passive transport prevails causing the foodstuff movement towards bed bottom and the effect of particle shape and size is highlighted. In fact, wide and planar shaped particles (like POd) descend by passive transport, but they can not ascend again in part because of roof effect, and in part due to the fact that particles are not able to enter into channels of small diameter. On the other hand, discs or spherical particles can be eventually actively transported when a channel is generated. Anyway, as it was demonstrated in experiments with 40 minutes of fluidization time (t40 cases), the downward movement prevails as time goes on.

With regard to the effect of food volumetric fraction, no general regular pattern can be observed for all the analyzed cases. For lyophilized carrots and potatoes (CAa and POa cases), a decrement of the segregation level is observed increasing food product volumetric fraction, while with peas (PEa cases) that parameter increases with food material concentration. At high velocity a possible explanation might be formulated taking into account the number of "weak zones" induced by the bigger solid and its shape. In the case of discs, for example, increasing foodstuff concentration the number of "weak zones" increases resulting in a greater number of channels. In addition, the planar shape and relatively small size might lead to a lower compaction of the material, and thus, passive transport globally compensates active transport resulting in a uniform mixing. On the opposite, spherical particles are actively transported easier than planar ones causing lower segregation levels than discs (as shown in Figure 8(b)). Thus, the greater concentration, the bigger number of "weak zones", and more foodstuff particles are actively transported inside the

channels.

Finally, Figure 9(b) shows a comparison between the L35b (fluidized bed) and the L20spjet (fluid-spout bed). It can be noted that whereas in the L35b the binary mixture is completely segregated for fresh product, the segregation level obtained in experiments performed in the L20spjet are considerably low (below 0.15) for all tested food materials. Moreover, TTSIS results of experiments carried out in the L20spjet (Table 7) exhibit a quite uniform distribution. Furthermore, in Table 6 it is possible to see that in L20spjet experiments tracer particles (both initially bottom and initially top tracers) exhibit uniform distributions in all the considered cases. These results evidence that food material is continuously distributed all along the bed during fluidization.

From the point of view of the previously mentioned transport mechanisms, the outcomes of experiments in the fluid-spout bed can be explained as follows. In the L20spjet only a central channel generated by the bed main injector is present, and its walls are constituted by compacted bran deposited by the fountain. Thus, food particles and adsorbent are transported actively in the central channel to bed surface, and passively in downward direction by bran in the annulus. Lateral air injectors avoid product concentration in bed bottom pushing it to the central channel, allowing an accurate mixing of the binary mixture.

4. CONCLUSIONS

In AFD by immersion in adsorbent material carried out in fluidized or spout-fluid bed, a good contact between the food material and the adsorbent is important to avoid the air saturation, taking advantage of the heat of adsorption for sublimating ice. Non-food wheat bran is a very promising material to be used as adsorbent. However, despite the fact that according to its population size distribution and EDF, it would be classified as a Geldart B powder, it fluidizes like a Geldart C. Thus, it

can be considered a "pseudo-cohesive" powder. This behavior may lead to potential difficulties in handling the binary mixture when the AFD process is carried out in a fluidized bed.

In addition, as it was expected from the theory, it was evidenced that, even for a binary mixture composed by a pseudo-cohesive powder and a solid whose particles are considerably greater than the powder ones, the air superficial velocity plays a very important role in mixing. Particularly, at high air flows (2.6 u_{mfA} for the analyzed cases) uniform distribution of the material of interest is reached when dried foodstuff is used. Nonetheless, product density plays a fundamental role, since nonuniform segregation profiles were obtained when fresh or partially lyophilized food material was considered, resulting in a poor contact between adsorbent and food material in the first stages of the AFD process in a fluidized bed.

Two food particle transport mechanisms (passive and active) and two movement blocking effects (floor and roof effects) were proposed to explain the observed behaviors. This, together with the Channel Generation and Collapse Cycle, permitted to explain the segregation phenomenon in channeling fluidized beds and the mixing process in fluid-spout beds.

Uniform mixing profiles were reached in the fluid-spout bed with a good circulation of the food particles along the bed during the fluidization. These results showed to be independent of the product density. Thus, this kind of bed should be used if an uniform mixing between adsorbent and food product is desired in the process of atmospheric freeze drying with use of adsorbent.

ACKNOWLEDGEMENTS

The present work was based on the PhD thesis of the corresponding author. The EUROTANGO Project (from the Erasmus Mundus Programme) is acknowledged for funding his PhD studies. In addition, the authors wish to thank Massimo Curti

and Giorgio Rovero for their practical help and recommendations in the fluidization field and equipment operation.

NOMENCLATURE

d	Food particle diameter	mm
d_{eq}	Equivalent Diameter for Fluidization (EDF)	m
d_{SV}	Sauter's diameter	mm
F_q	Accumulated mass of material of interest "q" from the bottom	kg
g	Gravity acceleration	m s^{-2}
h^*	Dimensionless position in the bed from the bottom	-
h_{bed}	Total bed height in settled state	m
Δh_i	Layer i thickness	m
Δh_i^*	Dimensionless thickness of layer	-
l, l_1, l_2, l_3	Food particle lengths	mm
m	Mass	kg
ΔP	Pressure drop	Pa
p_I	Bottom Third Indicator, in TTSIS (Equation 2)	-
p_M	Middle Third Indicator, in TTSIS (Equation 3)	-
p_S	Top Third Indicator, in TTSIS (Equation 4)	-

t, t_0	Time, and reference starting time	s
u	Air superficial velocity	m s^{-1}
u_{mf}	Minimum fluidization velocity	m s^{-1}
w_{PT}	Overall food product mass fraction	-

Greek Letters

μ	Air viscosity	Pa s
ρ	Density	kg m^{-3}
$\sigma_{\Delta P}$	Standard deviation of the pressure drop	Pa
σ_h	Standard deviation of the bed height	cm
ψ	Particle shape factor	-

Others

$\aleph_2$	Segregation level	-

Subscripts

A	Adsorbent (non-food wheat bran)	
air	Air	
b	Tracer particles initially in bed bottom	-
i	Layer i	
P	Food product	
q	Material of interest "q"	
T	Total	

t	Tracer particles initially in bed top	-

Acronyms

AFD Atmospheric Freeze Drying

EDF Equivalent Diameter for Fluidization

FB Fluidized Bed

IAM Immersion in an Adsorbent Medium

PSD Particle Size Distribution

TTSIS Three Thirds Segregation Index Set

VFD Vacuum Freeze Drying

REFERENCES

[1] Claussen, I.; Ustad, T.; Strømmen, I.; Walde, P. Atmospheric Freeze Drying - A Review. *Drying Technology* **2007,** *25(6)*, 947–957.

[2] Fissore, D.; Velardi, S. Freeze Drying: Basic Concepts and General Calculation Procedures. In *Operations in food refrigeration*; R. Mascheroni, Ed.; CRC Press - Taylor & Francis Group (CAN) , 2012, Chap. 3, pp. 47–70.

[3] Barresi, A.; Fissore, D. Freeze-drying equipments. In *Operations in food refrigeration*; R. Mascheroni, Ed.; CRC Press - Taylor & Francis Group (CAN) , 2012, Chap. 18, pp. 353–369.

[4] Eikevik, T. M.; Alves-Filho, O.; Bantle, M. Microwave-assisted atmospheric freeze drying of green peas: A case of study. *Drying Technology* **2012,** *30*, 1592–1599.

[5] Zielinska, M.; Zapotoczny, P.; Alves-Filho, O.; Eikevik, T. M.; Blaszczak, W. Microwave Vacuum-Assisted Drying of Green Peas Using Heat Pump and Fluidized Bed: A Comparative Study Between Atmospheric Freeze Drying and Hot Air Convective Drying. *Drying Technology* **2013,** *31(6)*, 633–642.

[6] Bantle, M.; Eikevik, T. M. Parametric study of high-intensity ultrasound in the atmospheric freeze drying of peas. *Drying Technology* **2011,** *29*, 1230–1239.

[7] Santacatalina, J.; Fissore, D.; Cárcel, J.; Mulet, A.; García-Pérez, J. Model-based investigation into atmospheric freeze drying assisted by power ultrasound. *Journal of Food Engineering* **2015,** *151*, 7–15.

[8] Pisano, R.; Fissore, D.; Barresi, A. Intensification of freeze-drying for the pharmaceutical and food industry. In *Modern Drying Technology Vol. 5: Process Intensification*; E. Tsotsas and A.S. Mujumdar, Ed.; Wiley-VCH Verlag GmbH & Co. KGaA: Weinhein , 2014, Chap. 5, pp. 131–161.

[9] Donsì, G.; Ferrari, G.; Di Matteo, P. Utilization of combined processes in freeze-drying of shrimps. *Food and bioproducts processing, Transactions of the Institution of Chemical Engineers, Part C* **2001,** *79(3)*, 152–159.

[10] Bustos, R.; Vásquez, M.; Vega, R.; Reyes, A.; Bubnovich, V.; Scheuermann, E. Comparative study of different process conditions of freeze drying of 'murtilla' berry. *Drying Technology* **2010,** *28*, 1416–1425.

[11] Boeh-Ocansey, O. Some factors influencing the freeze drying of carrot discs in vacuo and at atmospheric pressure. *Journal of Food Engineering* **1985,** *4*, 229–243.

[12] Reyes, A.; Mahn, A.; Huenulaf, P. Drying of apple slices in atmospheric and vacuum freeze dryer. *Drying Technology* **2011,** *29*, 1076–1089.

[13] Claussen, I.; Strømmen, I.; Hemmingsen, A. T.; Rustad, T. Relationship of product structure, sorption characteristics, and freezing point of atmospheric freeze-dried foods. *Drying Technology* **2007,** *25*, 853–865.

[14] Claussen, I.; Ansressen, T.; Eikevik, T.; Strømmen, I. Atmospheric freeze drying - Modeling and simulation of a tunnel dryer. *Drying Technology* **2007,** *25*, 1959–1965.

[15] Rahman, S.; Mujumdar, A. A novel atmospheric freeze drying system using a vibro-fluidized bed with adsorbent. *Drying Technology* **2008,** *26*, 393–403.

[16] Reyes, A.; Vega, R. V.; Bruna, R. D. Effect of Operating Conditions in Atmospheric Freeze Drying of Carrot Particles in a Pulsed Fluidized Bed. *Drying Technology* **2010,** *28*(10), 1185–1192.

[17] Duan, X.; Yang, X.; Ren, G.; Pang, Y.; Liu, L.; Liu, Y. Technical aspects in freeze-drying of foods. *Drying Technology* **2016,** *34*(11), 1271–1285.

[18] Donsì, G.; Di Matteo, P.; Ferrari, G. The role of heat and mass transfer phenomena in atmospheric freeze-drying of foods in a fluidised bed. *Journal of Food Engineering* **2003,** *59*, 267–275.

[19] Di Matteo, P. *Sviluppo di un processo per la liofilizzazione a pressione atmosferica di sostanze alimentari*. PhD thesis. Università degli Studi di Salerno, December 2002.

[20] Wolff, E.; Gibert, H. Atmospheric freeze-drying part 2: Modeling drying kinetics using adsorption isotherms. *Drying Technology* **1990,** *2*(8), 405–428.

[21] Rowe, P.; Nienow, A.; Agbim, A. The mechanisms by which particles segregate in gas fluidised beds - binary systems of near-spherical particles. *Transactions of the Institution of Chemical Engineers* **1972,** *50*(4), 310–323.

[22] Qiaoquna, S.; Huilina, L.; Wentiea, L.; Yuronga, H.; Lidana, Y.; Gidaspow, D. Simulation and experiment of segregating/mixing of rice husk-sand mixture in a bubbling fluidized bed. *Fuel* **2005,** *84*, 1739–1748.

[23] Wu, S.; Baeyens, J. Segregation by size difference in gas fluidized beds. *Powder Technology* **1998,** *98*, 139–150.

[24] Chew, J.; Hrenya, C. Link between bubbling and segregation patterns in gas-fluidized beds with continuous size distributions. *AIChE Journal* **2011,** *57*(11), 3003–3011.

[25] Geldart, D. Types of gas fluidization. *Powder Technology* **1973,** *7*, 285–292.

[26] Bi, H. T. A critical review of the complex pressure fluctuation phenomenon in gas–solids fluidized beds. *Chemical Engineering Science* **2007,** *62*(13), 3473–3493.

[27] Visser, J. van der Waals and other cohesive forces affecting powder fluidization. *Powder Technology* **1989,** *1*, 1–10.

[28] Geldart, D.; Harnby, N.; Wong, A. Fluidization of cohesive powders. *Powder Technology* **1984,** *31*(1), 25–37.

[29] Wright, P.; Raper, J. Role of liquid bridge forces in cohesive fluidization. *Transactions of the Institution of Chemical Engineers, Part A* **1998,** *76*, 753–760.

[30] Sundaresan, S. Instabilities in fluidized beds. *Annual Review of Fluid Mechanics* **2003,** *35*, 63–88.

[31] Zhou, T.; Li, H. Estimation of agglomerate size for cohesive particles during fluidization. *Powder Technology* **1999,** *101*, 57–62.

[32] van Wachem, B.; Sasic, S. Derivation, simulation and validation of a cohesive particle flow CFD model. *AIChe Journal* **2008,** *54*(1), 9–19.

[33] Sutanto, W. *Hydrodynamics of spout fluid beds*. PhD thesis. University of British Columbia, July 1981.

[34] Zhang, Y.; Zhong, W.; Jin, B.; Xiao, R. Mixing and segregation behavior in a spout-fluid bed: effect of particle size. *Industrial and Engineering Chemistry Research* **2012,** *51*, 14247–14257.

[35] Du, W.; Zhang, L.; Zhang, B.; Bao, S.; Xu, J.; Wie, W. Pressure drop and pressure fluctuations in spouted beds with binary mixtures of particles. *Powder Technology* **2015,** *276*, 134–143.

[36] Kumar, B.; Vinod, A. Mixing characteristics of binary mixtures in a spout-fluid bed. *Particulate Science and Technology* **2016,** In press. DOI: 10.1080/02726351.2016.1146810.

[37] Zhang, Y.; Zhong, W.; Jin, B.; Xiao, R. Mixing and segregation behavior in a spout-fluid bed: effect of particle density. *Industrial and Engineering Chemistry Research* **2013,** *52*, 5489–5497.

[38] Passos, M. L.; Mujumdar, A. S.; Vijaya, G.; Raghavan, V. G. Spouted and spout-fluidized beds for gram drying. *Drying Technology* **1989,** *7*(4), 663–696.

[39] Lima, A. C. C.; Rocha, S. C. S. Bean drying in fixed, spouted and spout-fluid beds: a comparison and empirical modeling. *Drying Technology* **1998,** *16*(9-10), 1881–1901.

[40] Zhong, W.; Chen, X.; Zhang, M. Hydrodynamic characteristics of spout-fluid bed: Pressure drop and minimum spouting/spout-fluidizing velocity. *Chemical Engineering Journal* **2006,** *118*(1–2), 37–46.

[41] Link, J.; Cuypers, L.; Deen, N.; Kuipers, J. Flow regimes in a spout–fluid bed: A combined experimental and simulation study. *Chemical Engineering Science* **2005,** *60*(13), 3425–3442.

[42] Zhang, J.; Tang, F. Prediction of flow regimes in spout-fluidized beds. *China Particuology* **2006,** *4*(3–4), 189–193.

[43] Zhong, W.; Zhang, M.; Jin, B.; Yuan, Z. Three-dimensional simulation of gas/solid flow in spout-fluid beds with kinetic theory of granular flow. *Chinese Journal of Chemical Engineering* **2006,** *14*(5), 611–617.

[44] Wang, S.; Zhao, L.; Wang, C.; Liu, Y.; Gao, J.; Liu, Y.; Cheng, Q. Numerical simulation of gas–solid flow with two fluid model in a spouted-fluid bed. *Particuology* **2014,** *14*, 109–116.

[45] Coletto, M. *Atmospheric freeze drying of food in fluidized beds - Practical aspects and CFD simulation*. PhD thesis. Politecnico di Torino, February 2015. DOI: 10.6092/polito/porto/2588248.

[46] Coletto, M.; Marchisio, D.; Barresi, A. A new segregation index for solid multicomponent mixtures. *Powder Technology* **2016,** *299*, 77–86.

[47] Wormsbecker, M.; Pugsley, T. The influence of moisture on the fluidization behaviour of porous pharmaceutical granule. *Chemical Engineering Science* **2008,** *63*, 4063–4069.

[48] Zhou, H.; Xiong, Y.; Pei, Y. Effect of moisture content on dense-phase pneumatic conveying of pulverized lignite under high pressure. *Powder Technology* **2016,** *287*, 355–363.

[49] Makkawi, Y.; Wright, P. Tomographic analysis of dry and semi-wet bed fluidization: the effect of small liquid loading and particle size on the bubbling behaviour. *Chemical Engineering Science* **2004,** *59*, 201–213.

[50] McLaughlin, L.; Rhodes, M. Prediction of fluidized bed behaviour in the presence of liquid bridges. *Powder Technology* **2001,** *114*, 213–223.

[51] Malek, M.; Benjamin, C.; Lu, Y. Pressure drop and spoutable bed height in spouted beds. *I&EC Process Design and Development* **1965,** *4*(1), 123–128.

[52] van Ommen, J.; de Corte, R.; van den Bleek, C. Rapid detection of defluidization using the standard deviation of pressure fluctuations. *Chemical Engineering and Processing* **2004,** *43*, 1329–1335.

[53] Gómez-Hernández, J.; Soria-Verdugo, A.; Villa Briongos, J.; Santana, D. Fluidized bed with a rotating distributor operated under defluidization conditions. *Chemical Engineering Journal* **2012,** *195–196*, 198–207.

[54] Serrano, D.; Sánchez-Delgado, S.; Sobrino, C.; Marugán-Cruz, C. Defluidization and agglomeration of a fluidized bed reactor during *Cynara cardunculus* L. gasification using sepiolite as a bed material. *Fuel Processing Technology* **2015,** *131*, 331–347.

[55] van Ommen, J.; Srdjan, S.; van der Schaaf, J.; S., G.; Johnsson, F.; Marc-Olivier, C. Time-series analysis of pressure fluctuations in gas-solid fluidized beds - A review. *International Journal of Multiphase Flow* **2011,** *37*, 403–428.

TABLES

TABLE 1: Utilized food material with its shape characteristics.

Code	Material	Particle shape	Dimensions (mm)	d_{SV} (mm)	ψ	ρ (kg/m^3)
CAf	fresh carrot	disc	l=5.0, d=35.0	11.7	0.557	1050±55
CAa	lyophilized carrot	disc	l=5.0, d=18.0	9.5	0.719	158±8
CAb	lyophilized carrot	disc	l=5.0, d=21.0	10.2	0.681	112±6
POa	lyophilized potato	slab	l_1=l_2=12.5, l_3=5.0	8.3	0.729	176±11
POb	fresh potato1	cube	l=10.0	10.0	0.806	1070±13
POc	fresh potato2	slab	l_1=l_2=12.5, l_3=5.0	8.3	0.729	1070±13
POd	lyophilized potato	slab	l_1=l_2=40.0, l_3=5	12.0	0.484	198±8
PEa	liophilized pea	sphere	d=8.8	8.8	1.000	202±7
PEb	partially-lyophilized pea	sphere	d=8.8	8.8	1.000	401±14
PEc	liophilized pea	sphere	d=8.8	8.8	1.000	237±8
PEf	fresh pea	sphere	d=8.8	8.8	1.000	1088±37

TABLE 2: Type of fluidized bed used (ID code, characteristics and experiments done in each one).

ID	Section shape	Base dimensions (mm)	Other characteristics	Experiments done
L35b	square	350x350	-	bran hydrodynamics; segregation and mixing
L20b	square	200x200	-	bran hydrodynamics
L065b	circle	65	cylindrical	bran hydrodynamics
L20spjet	rectangle	200x100	spout-fluid bed	segregation and mixing

bran hydrodynamics: hydrodynamic study of non-food wheat bran alone

TABLE 3: Conditions for performed experiments in the L35b fluidized bed and in the spout-fluid bed (identified by "L20spjet").

Experiment ID	Air flow (m^3/h)	Material	w_{PT}	u/u_{mfA}
POd0260R40t20	210	lyophilized potato	0.0046	2.75
POd0170R40t20	130	lyophilized potato	0.0046	1.70
POd0150R40t20	120	lyophilized potato	0.0046	1.54
POa0150R40t10	120	lyophilized potato	0.0035	1.47
POa0150R80t10	120	lyophilized potato	0.0016	1.47
POa0170R40t10	140	lyophilized potato	0.0036	1.82
POa0170R80t10	140	lyophilized potato	0.0017	1.71
PEb0260R20t20	200	partially lyophilized pea	0.0138	2.57
PEb0170R80t20	140	partially lyophilized pea	0.0039	1.75
PEa0260R20t20	200	lyophilized pea	0.0093	2.57
PEa0260R80t20	200	lyophilized pea	0.0023	2.56
PEc0230R20t20	175	lyophilized pea	0.0109	2.42
PEc0190R20t20	145	lyophilized pea	0.0109	1.93
PEa0150R20t20	120	lyophilized pea	0.0089	1.49
PEa0150R80t20	120	lyophilized pea	0.0024	1.49
CAa0260R20t20	200	lyophilized carrot	0.0069	2.60
CAa0260R40t20	200	lyophilized carrot	0.0033	2.60
CAa0260R80t20	200	lyophilized carrot	0.0012	2.59
CAb0190R20t20	145	lyophilized carrot	0.0053	1.85
CAa0170R20t20	140	lyophilized carrot	0.0060	1.75
CAa0170R40t20	140	lyophilized carrot	0.0032	1.76
CAa0170R80t20	140	lyophilized carrot	0.0014	1.76
CAa0150R20t20	120	lyophilized carrot	0.0067	1.50
CAa0150R40t20	120	lyophilized carrot	0.0034	1.49
CAa0150R80t20	120	lyophilized carrot	0.0013	1.50
CAb0150R20t40	120	lyophilized carrot	0.0053	1.57
CAb0170R20t40	130	lyophilized carrot	0.0053	1.66
CAb0260R20t40	200	lyophilized carrot	0.0053	2.69
PEcR20L20spjet	37	lyophilized pea	0.0109	0.51*
PEfR20L20spjet	37	fresh pea	0.0500	0.51*
CAbR20L20spjet	37	lyophilized carrot	0.0053	0.51*
CAdR20L20spjet	37	fresh carrot	0.0500	0.51*

**Velocity of experiments performed in the L20spjet is not the relative air velocity u/u_{mfA}, but the absolute velocity, u (m/s).*

TABLE 4: Results in terms of TTSIS for segregation experiments in the L35b with 20 min of fluidization time.

Experiment	p_I	p_M	p_S	$\aleph_2$	Segregation type
POd0260R40t20	0.335	0.186	0.479	0.293	V-Top
POd0170R40t20	0.899	0.101	0.000	0.899	Bottom
POd0150R40t20	0.724	0.221	0.055	0.668	Bottom
POa0170R80t10	0.185	0.180	0.635	0.455	Top
POa0170R40t10	0.253	0.371	0.375	0.122	Top Central
POa0150R80t10	0.000	0.011	0.989	0.989	Full Top
POa0150R40t10	0.000	0.118	0.882	0.882	Top
PEb0260R20t20	0.715	0.155	0.129	0.586	Bottom
PEb0170R80t20	0.758	0.202	0.040	0.717	Bottom
PEa0260R80t20	0.322	0.339	0.339	0.017	Uniform
PEa0260R20t20	0.273	0.354	0.372	0.099	Top Central
PEc0230R20t20	0.399	0.274	0.328	0.125	V-Bottom
PEc0190R20t20	0.411	0.255	0.334	0.156	V-Bottom
PEa0150R80t20	0.240	0.371	0.389	0.149	Top Central
PEa0150R20t20	0.274	0.436	0.291	0.162	Central Top
CAa0260R80t20	0.242	0.351	0.407	0.165	Top Central
CAa0260R40t20	0.292	0.336	0.372	0.080	Top Central
CAa0260R20t20	0.305	0.357	0.338	0.053	Uniform
CAb0190R20t20	0.544	0.265	0.191	0.354	Bottom Central
CAa0170R80t20	0.612	0.289	0.099	0.513	Bottom
CAa0170R40t20	0.567	0.272	0.161	0.407	Bottom
CAa0170R20t20	0.299	0.475	0.226	0.249	Central Bottom
CAa0150R80t20	0.091	0.496	0.413	0.405	Central Top
CAa0150R40t20	0.206	0.377	0.417	0.212	Top Central
CAa0150R20t20	0.240	0.430	0.330	0.190	Central Top

TABLE 5: Results in terms of TTSIS for segregation experiments in the L35b with 40 min of fluidization time.

Experiment	p_I	p_M	p_S	$\aleph_2$	Segregation type
CAb0150R20t40	0.682	0.228	0.090	0.591	Bottom
CAb0170R20t40	0.521	0.331	0.147	0.374	Bottom Central
CAb0260R20t40	0.313	0.340	0.346	0.033	Uniform

TABLE 6: Results in terms of TTSIS of tracer particles of segregation experiments presented in Tables 4, 5, and 7.

Experiment	Bottom tracers			Top tracers		
	p_{I_B}	p_{M_B}	p_{S_B}	p_{I_T}	p_{M_T}	p_{S_T}
CAb0190R20	0.822	0.072	0.106	0.221	0.464	0.315
POd0150R40	0.838	0.157	0.005			
POd0170R40	0.937	0.063	0.000	0.829	0.171	0.000
POd0260R40	0.402	0.176	0.422	0.079	0.209	0.712
PEc0190R20	0.000	0.000	1.000	0.393	0.324	0.283
PEc0230R20	0.518	0.204	0.278	0.240	0.292	0.467
CAb0150R20t40	0.950	0.050	0.000	0.609	0.238	0.152
CAb0170R20t40	0.852	0.074	0.074	0.448	0.320	0.232
CAb0260R20t40	0.488	0.315	0.196	0.118	0.444	0.438
PEcR20L20spjet	0.326	0.268	0.407	0.211	0.347	0.442
PEfR20L20spjet	0.339	0.393	0.268	0.263	0.362	0.375
CAdR20L20spjet	0.267	0.327	0.407	0.323	0.359	0.319
CAdR20L20spjet	0.564	0.228	0.208	0.309	0.311	0.379

TABLE 7: Results in terms of TTSIS for segregation experiments in the L20spjet with 20 min of fluidization time.

Experiment	p_I	p_M	p_S	$\aleph_2$	Segregation type
PEcR20L20spjet	0.265	0.330	0.405	0.140	Top Central
PEfR20L20spjet	0.292	0.373	0.334	0.081	Central Top
CAdR20L20spjet	0.272	0.339	0.389	0.117	Top Central
CAbR20L20spjet	0.403	0.298	0.299	0.105	V-Bottom

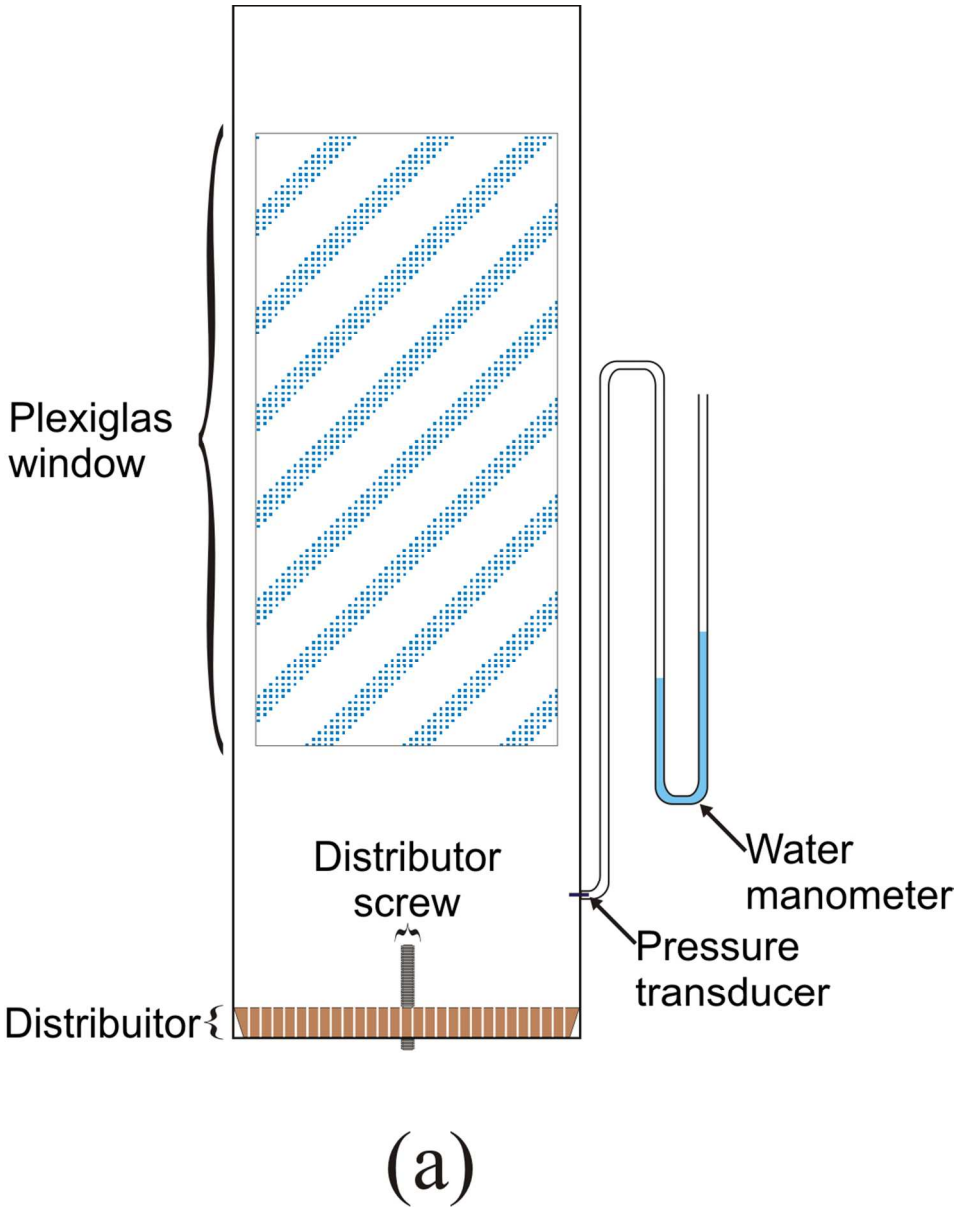

FIG.1: Utilized beds. (a) L35b (350 mm sided fluidized bed). L20b is similar but smaller and its plexiglas window extends to all the bed height. (b) L20spjet (200 mm spout-fluid bed).
Figure 1(a)
97x123mm (300 x 300 DPI)

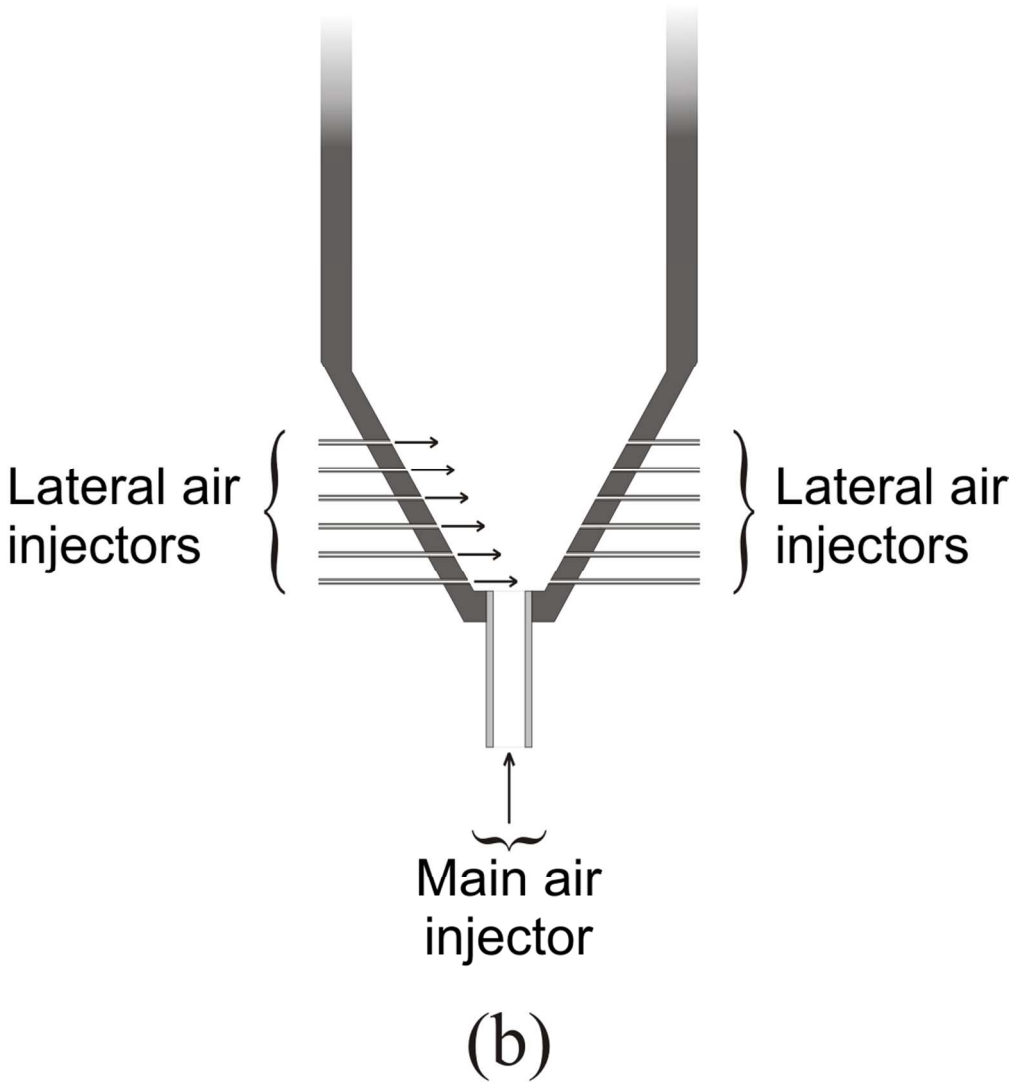

FIG.1: Utilized beds. (a) L35b (350 mm sided fluidized bed). L20b is similar but smaller and its plexiglas window extends to all the bed height. (b) L20spjet (200 mm spout-fluid bed).
Figure 1(b)
94x105mm (300 x 300 DPI)

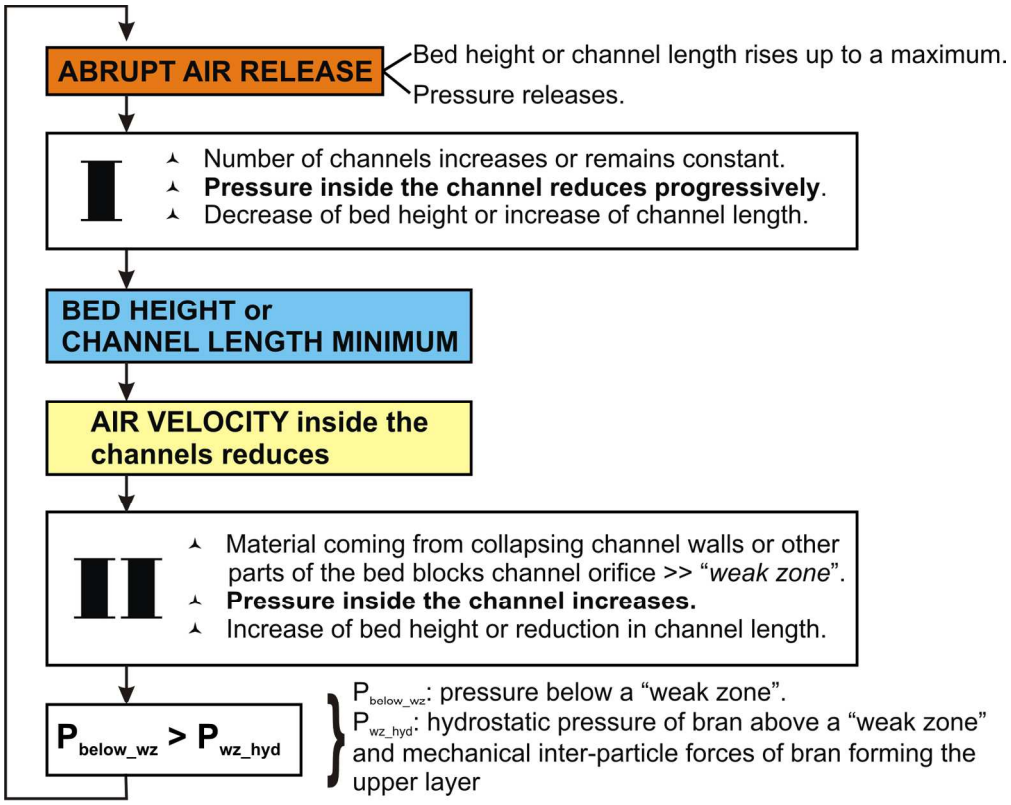

FIG.2: Channels generation (I) and collapse (II) general cycle.

149x119mm (300 x 300 DPI)

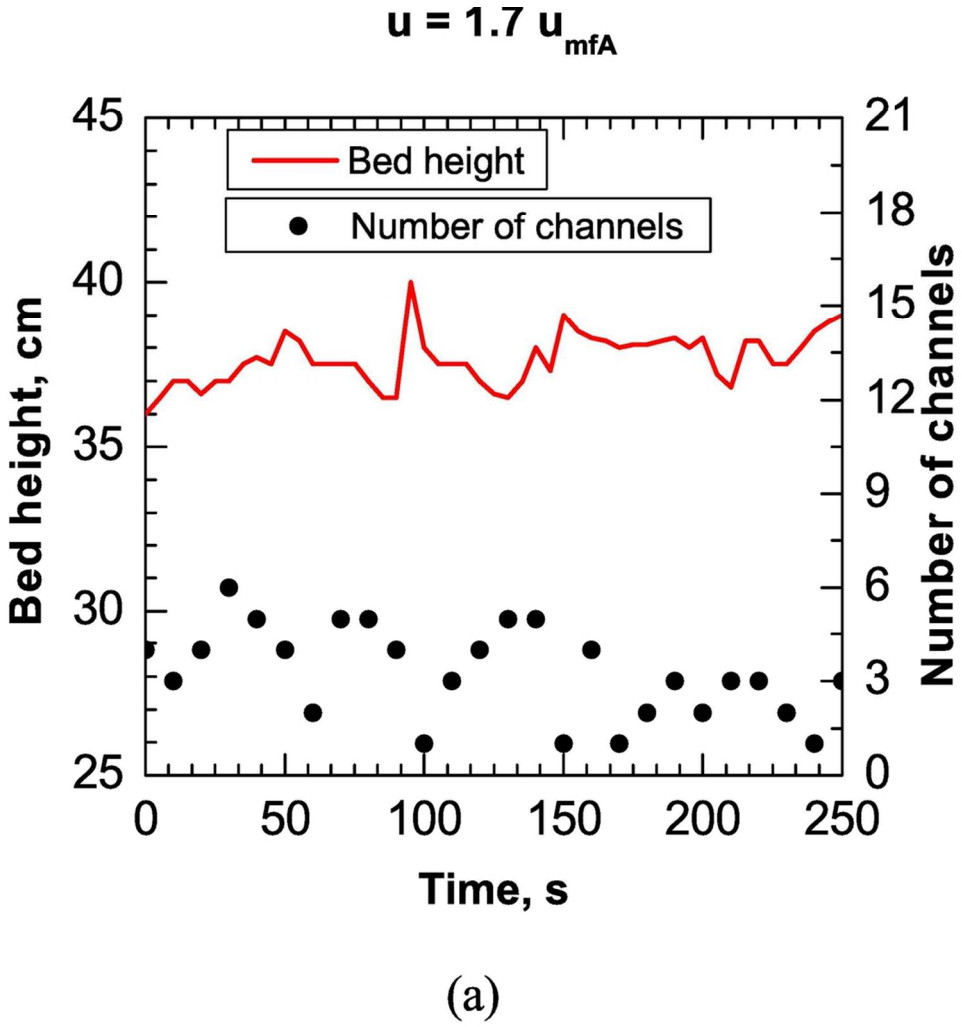

(a)

FIG. 3: Number of channels and bed height at different air superficial velocities (in L35b fluidized bed).

98x101mm (300 x 300 DPI)

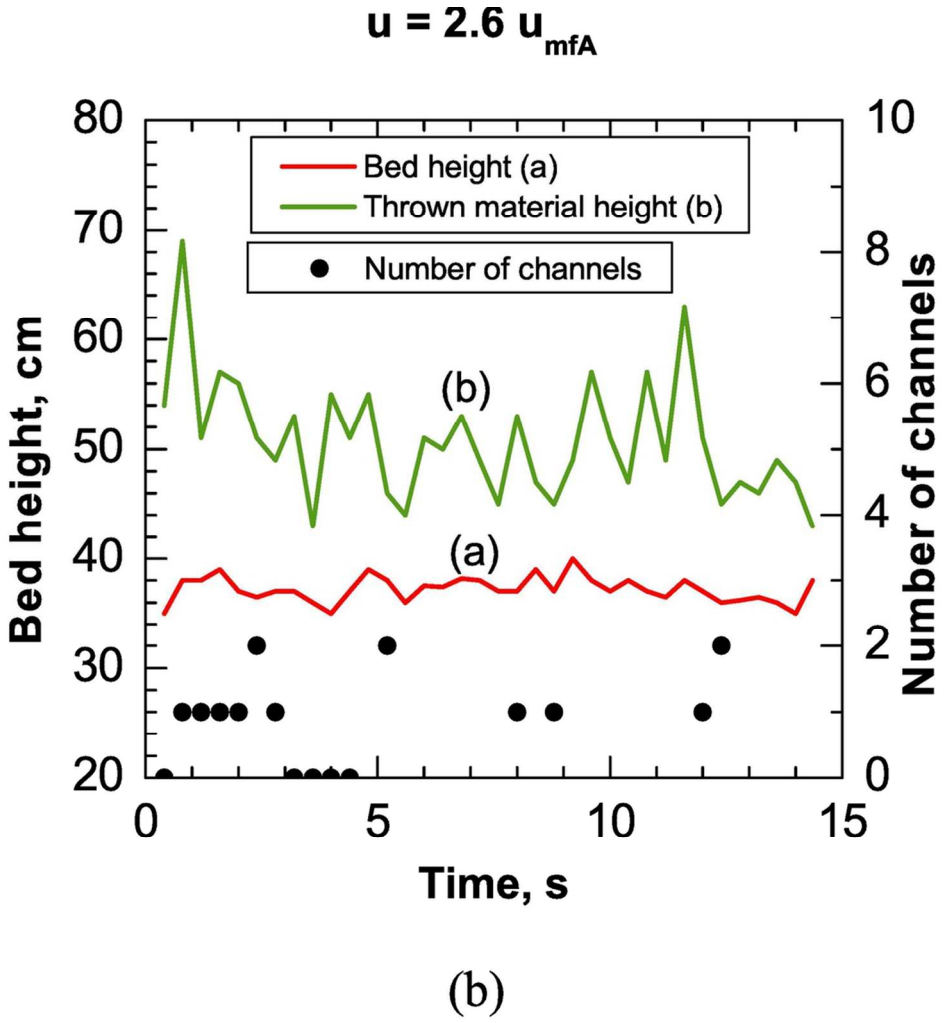

(b)

FIG. 3: Number of channels and bed height at different air superficial velocities (in L35b fluidized bed).

98x101mm (300 x 300 DPI)

t = 49.0 s

t = 50.4 s

t = 51.0 s

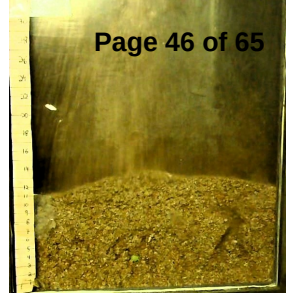

t = 51.4 s

t = 52.2 s

t = 53.0 s

t = 54.2 s

t = 61.4 s

t = 91.8 s t = 92.4 s t = 92.9 s t = 93.7 s t = 99.7 s

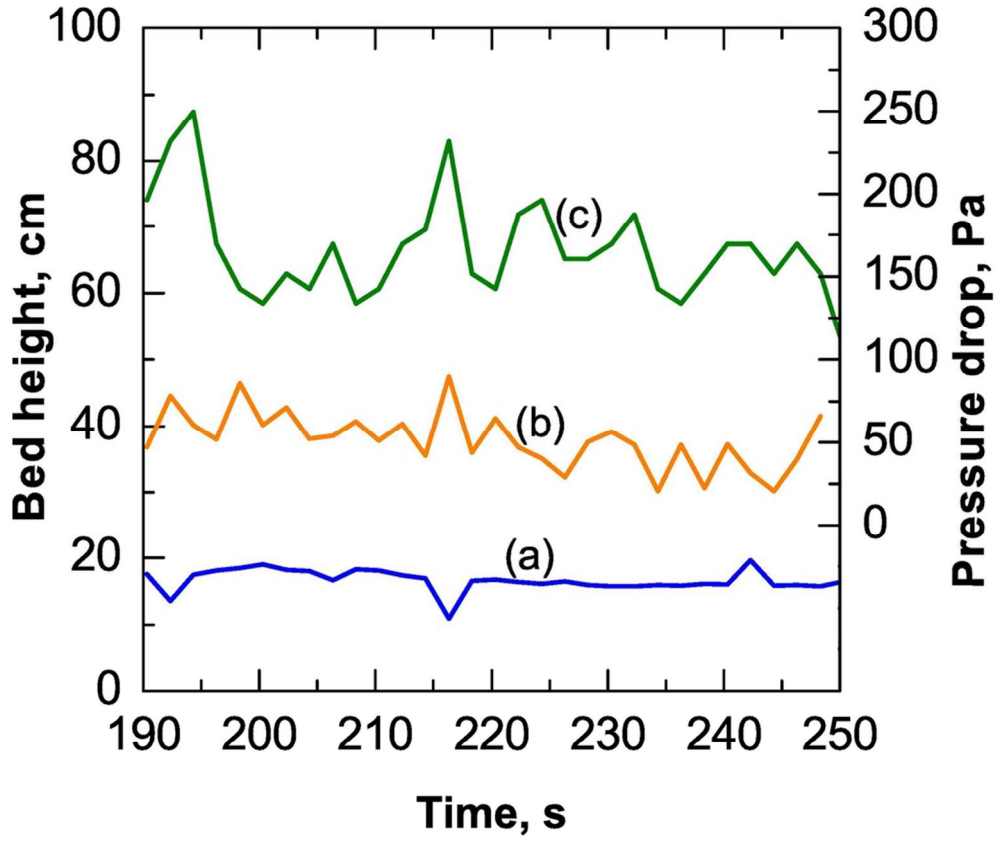

FIG. 6: Oscillations of pressure drop (c), bed height (a), and height of thrown material (fountain) (b) during bran fluidization in the L065b bed.

88x82mm (300 x 300 DPI)

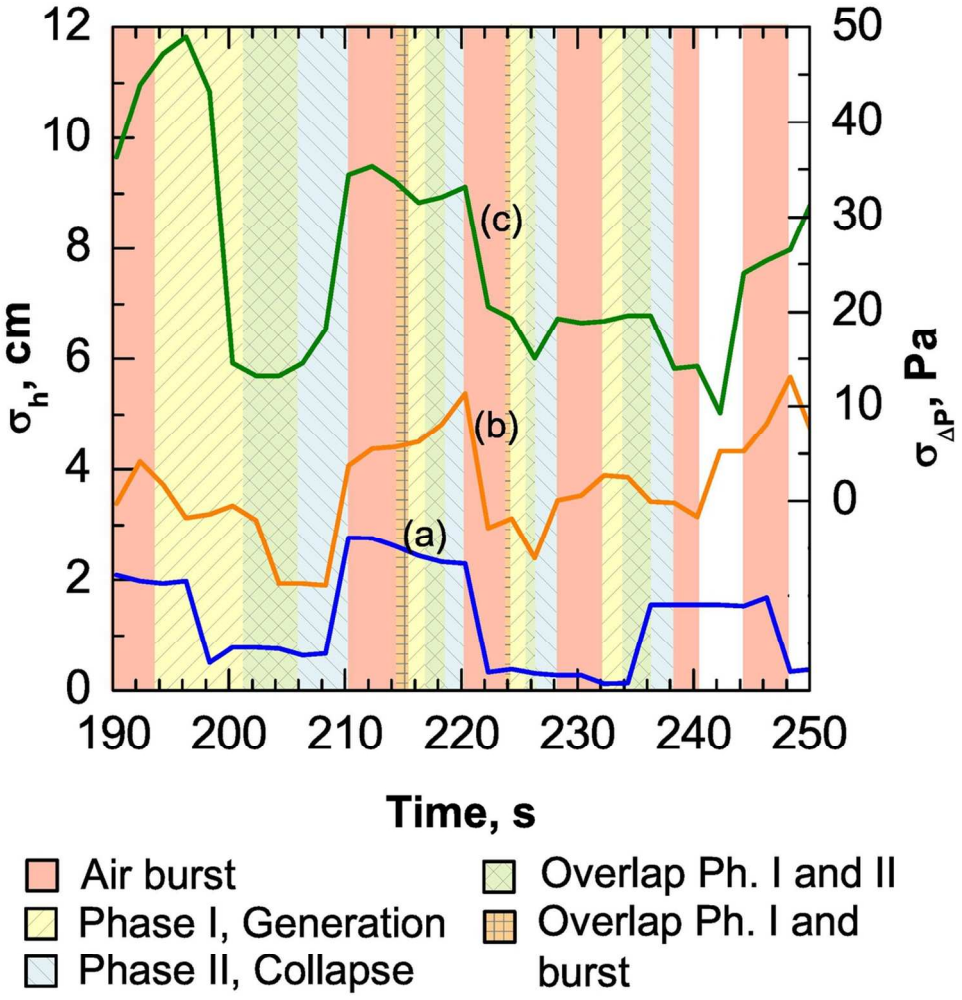

FIG. 7: Standard deviations of the pressure drop (c), bed height (a), and height of thrown material (fountain) (b) presented in Figure 6. The phases of the channel generation and collapse cycles are evidenced.

108x123mm (300 x 300 DPI)

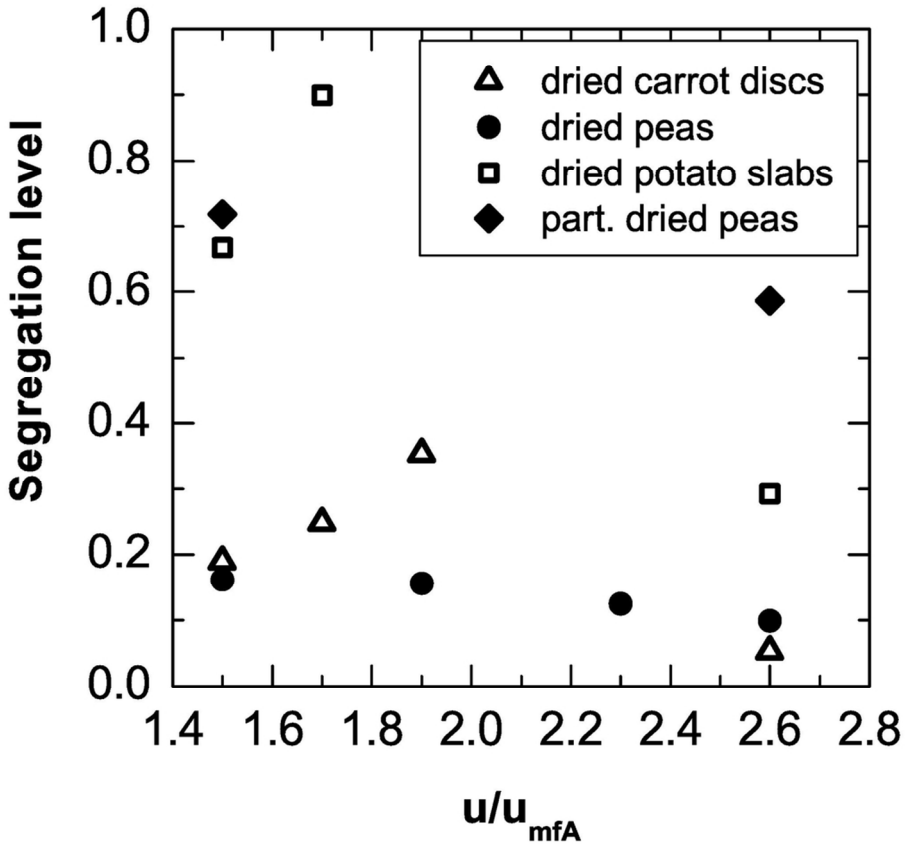

(a)

FIG. 8: Effects of air superficial velocity and concentration on segregation in the L35b fluidized bed. (a) Segregation level as function of air superficial velocity relative to bran mininum fluidization velocity. Concentrations: R40 for dried potato slabs cases, R20 for the other ones. (b) Segregation level in terms of equivalent fresh product to adsorbent mass ratio (see Tables 1 and 3 for experiment and product code).

98x101mm (300 x 300 DPI)

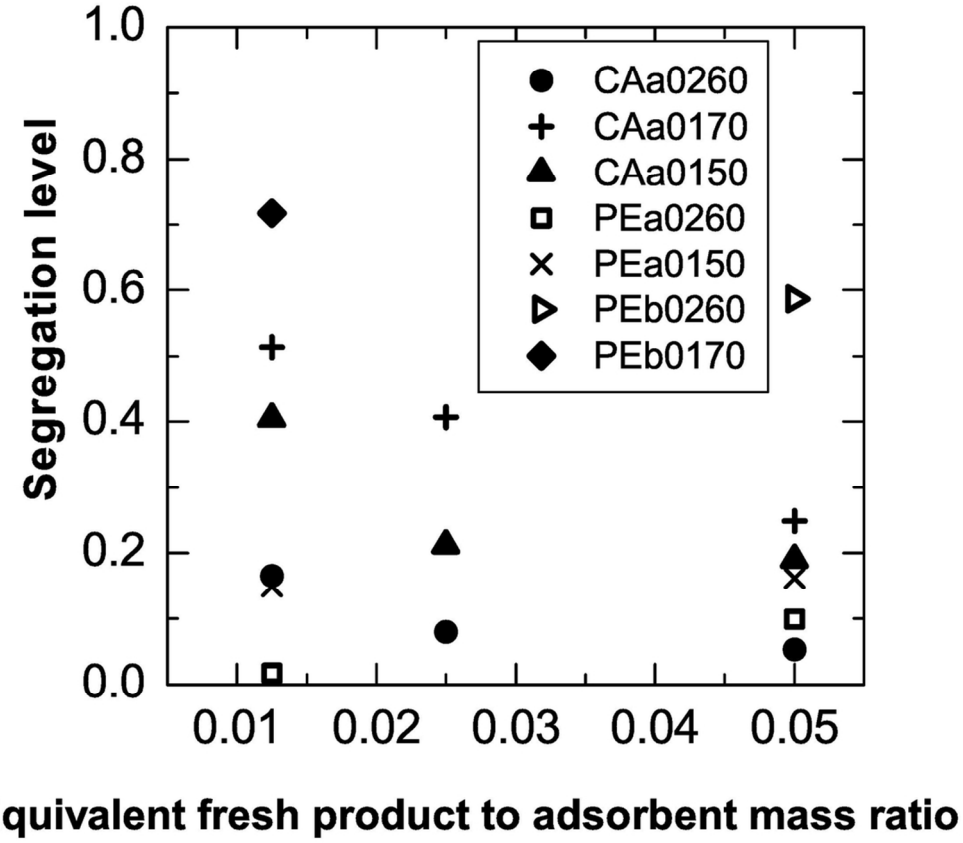

(b)

FIG. 8: Effects of air superficial velocity and concentration on segregation in the L35b fluidized bed. (a) Segregation level as function of air superficial velocity relative to bran mininum fluidization velocity. Concentrations: R40 for dried potato slabs cases, R20 for the other ones. (b) Segregation level in terms of equivalent fresh product to adsorbent mass ratio (see Tables 1 and 3 for experiment and product code).

98x101mm (300 x 300 DPI)

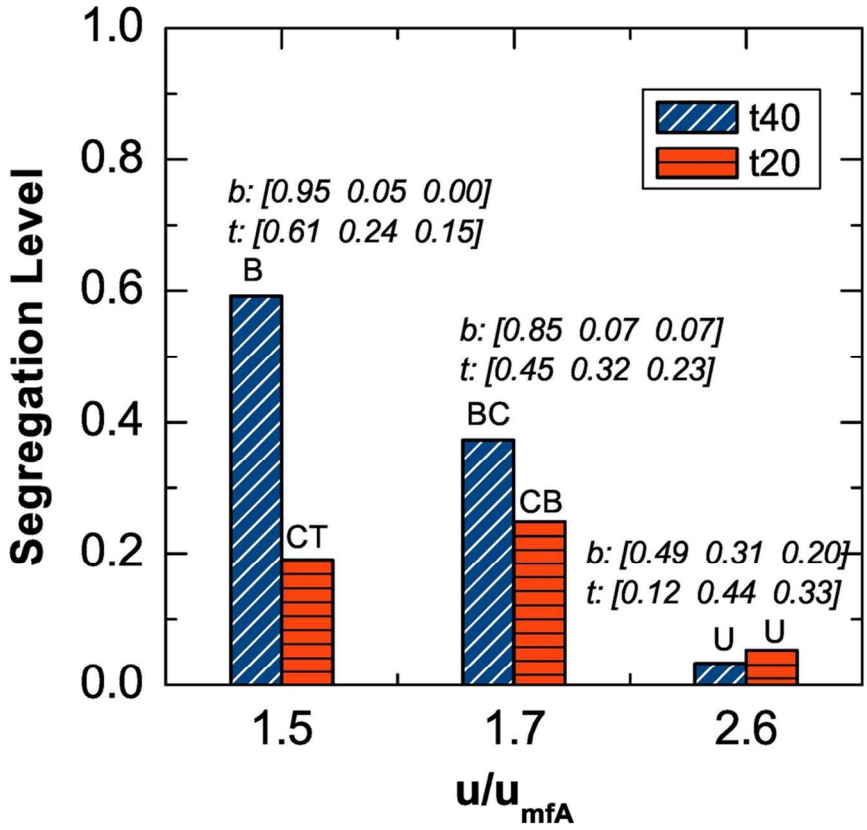

(a)

FIG. 9:Fluidization time and performance of two different beds. (a) Effect of fluidization time on segregation as a funtion of relative air superficial velocity. Food material: lyophilized carrot discs (CAa, CAb). TTSIS for tracer particles corresponds to t40 experiments (iB: initially in bottom, iT: initially in top). (b) Performance of the fluidized bed (L35b) and the spout-fluid bed (L20spjet) for dried and fresh foodstuff. 20 minutes of fluidization time. Concentration: R20. Air superficial velocity in the L35b: 2.6 $u_{\nm{mfA}}$.

98x101mm (300 x 300 DPI)

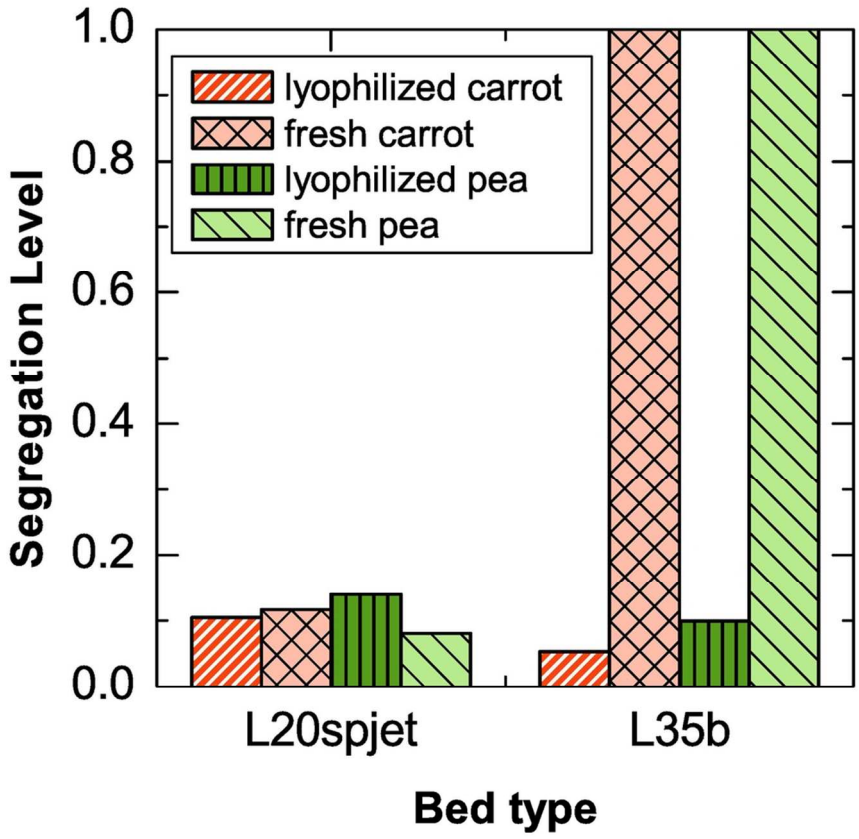

(b)

FIG. 9:Fluidization time and performance of two different beds. (a) Effect of fluidization time on segregation as a funtion of relative air superficial velocity. Food material: lyophilized carrot discs (CAa, CAb). TTSIS for tracer particles corresponds to t40 experiments (iB: initially in bottom, iT: initially in top). (b) Performance of the fluidized bed (L35b) and the spout-fluid bed (L20spjet) for dried and fresh foodstuff. 20 minutes of fluidization time. Concentration: R20. Air superficial velocity in the L35b: 2.6 $u_{\nm{mfA}}$.

98x101mm (300 x 300 DPI)

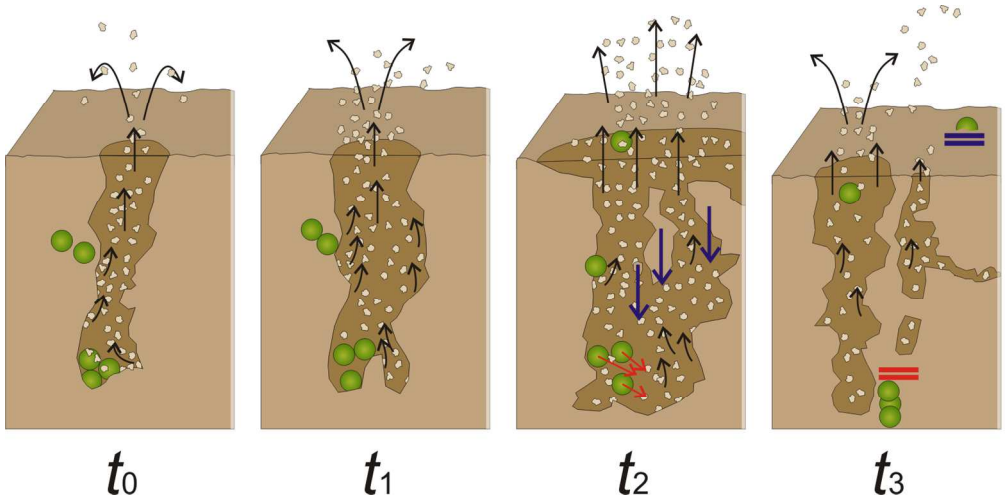

FIG. 10: Passive transport and blocking effects, during the generation (or expansion) and collapse of a channel. Bran is dragged by air from channel walls producing cavities under food particles (t_{0}), and leading to they displacement (t_{1}). After an air burst, some food particles move towards the new generated space (t_{2}, red arrows), and simultaneously, bran from the collapsing channel walls covers the recently deposited food particles (blue arrows). Finally, food particles in the channel bottom are completely covered by bran and their upwards movement is blocked by roof effect (t_{3}). In addition, the downward movement of a deposited particle on the bed surface is blocked by floor effect. Also some particles may be actively transported during the channel generation-collapse process ($t_{2} $ and t_{3}).

139x68mm (300 x 300 DPI)

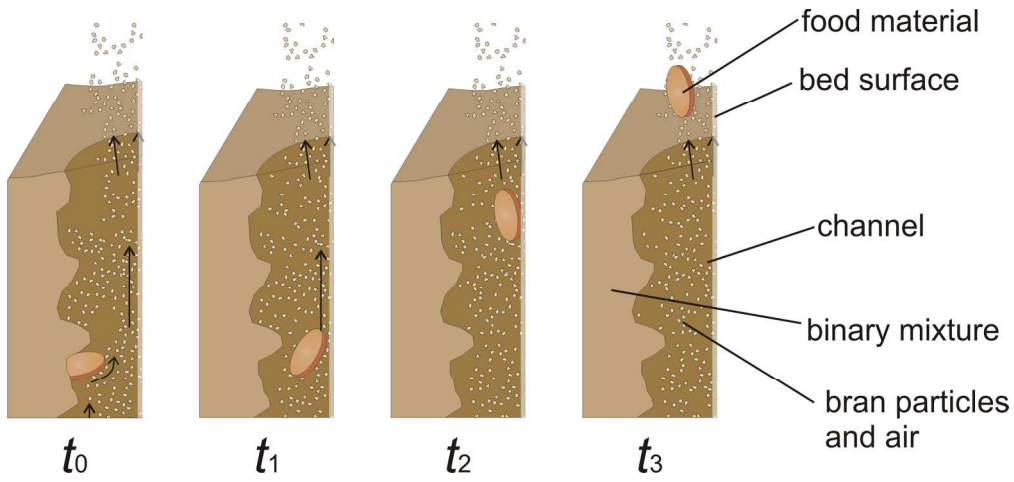

FIG. 11: Active transport of a food particle. At t_{0} bran particles are dragged by air, impacting on the grater particle surface and transferring their momentum. Then, the food particle is moved from its embedded position, and dragged by air.

171x79mm (300 x 300 DPI)